Mutagenesis, 2018, XX, 1–7
doi:10.1093/mutage/gey021
Original Manuscript

Original Manuscript

Investigating FlowSight® imaging flow cytometry as a platform to assess chemically induced micronuclei using human lymphoblastoid cells *in vitro*

Jatin R. Verma[1,*], Danielle S. G. Harte[1], Ume-Kulsoom Shah[1], Huw Summers[3], Catherine A. Thornton[1], Shareen H. Doak[1], Gareth J. S. Jenkins[1], Paul Rees[3], John W. Wills[2,†] and George E. Johnson[1,†]

[1]Institute of Life Science, Swansea University Medical School, Swansea University, Swansea SA2 8PP, [2]Department of Veterinary Medicine, School of Biological Sciences, University of Cambridge, Cambridge, CB3 0ES and [3]College of Engineering, Swansea University, Swansea SA1 8EN

*To whom correspondence should be addressed. Email: Jatin_verma12@yahoo.com

[†]Authors contributed equally to the project

Received 3 April 2018; Revised 5 July 2018; Editorial decision 23 July 2018; Accepted 31 August 2018.

Abstract

Use of imaging flow cytometry to assess induced DNA damage via the cytokinesis block micronucleus (CBMN) assay has thus far been limited to radiation dosimetry in human lymphocytes using high end, 'ImageStream X' series imaging cytometers. Its potential to enumerate chemically induced DNA damage using *in vitro* cell lines remains unexplored. In the present manuscript, we investigate the more affordable FlowSight® imaging cytometry platform to assess *in vitro* micronucleus (MN) induction in the human lymphoblastoid TK6 and metabolically competent MCL-5 cells treated with Methyl Methane Sulfonate (MMS) (0–5 μg/ml), Carbendazim (0–1.6 μg/ml), and Benzo[a]Pyrene (B[a]P) (0–6.3 μg/ml) for a period of 1.5–2 cell-cycles. Cells were fixed, and nuclei and MN were stained using the fluorescent nuclear dye DRAQ5™. Image acquisition was carried out using a 20X objective on a FlowSight® imaging cytometer (Amnis, part of Merck Millipore) equipped with a 488 nm laser. Populations of ~20 000 brightfield cell images, alongside DRAQ5™ stained nuclei/MN were rapidly collected (≤10 min). Single, in-focus cells suitable for scoring were then isolated using the IDEAS® software. An overlay of the brightfield cell outlines and the DRAQ5 nuclear fluorescence was used to facilitate scoring of mono-, bi-, tri-, and tetra-nucleated cells with or without MN events and in context of the cytoplasmic boundary of the parent cell.

To establish the potential of the FlowSight® platform, and to establish 'ground truth' cell classification for the supervised machine learning based scoring algorithm that represents the next stage of our project, the captured images were scored manually. Alongside, MN frequencies were also derived using the 'gold standard' light microscopy and manual scoring. A minimum of 3000 bi-nucleated cells were assessed using both approaches. Using the benchmark dose approach, the comparability of genotoxic potency estimations for the different compounds and cell lines was assessed across the two scoring platforms as highly similar. This study therefore provides essential proof-of-concept that FlowSight® imaging cytometry is capable of reproducing the results of 'gold standard' manual scoring by light microscopy. We conclude that, with the right automated scoring algorithm, imaging flow cytometry could revolutionise the reportability and scoring throughput of the CBMN assay.

Introduction

The *in vitro* micronucleus (MN) assay is a gold-standard test used worldwide to assess substances' ability to cause DNA damage and chromosomal aberration. MN formation resulting from either chromosomal breaks or chromosomal loss is used as a measure of induced DNA damage. The MN assay is mandated by regulatory authorities as a robust genetic toxicity screening tool (1,2). Scoring slides using light microscopy is the conventional approach to detect cell with MN, as the method is simple, economical and is currently considered the 'gold standard' for MN scoring (3). However, this method is also associated with being low throughput and biased by potential scorer-subjectivity and extensive scoring time (4,5). A variety of automated MN scoring platforms have therefore been developed in an attempt to obtain high-content, high throughput MN scores with reduced subjectivity.

To date, most automated MN scoring approaches have employed automatic slide-scanning microscopy in conjunction with object-based image classification or else have employed conventional flow cytometry (4,6,7). Commercially available automated microscopy platforms such as the Metafer™ (MetaSystems, Newton, USA) enable rapid MN scoring (8). However, lack of cytoplasmic staining, limitations of the current image analysis classifiers in the detection of overlapping nuclei/MN, the need for optimisation of the classifier setting for new chemicals, and the importance of high quality of slide preparations have been identified as issues with this platform (9,10). In contrast, fully automated flow cytometry based MN scoring platforms provide an advantage over microscopy based approaches in terms of high-throughput, rapid assessment of MN events (11). However, the fact these approaches typically lyse cells and score the resultant, mixed population of nuclei and micronuclei has led to concerns such as over-scoring of the MN events due to misclassification of apoptotic bodies/debris (12).

FlowSight® and ImageStream X MarkII® (Amnis, part of Merck Millipore) are examples of commercially available imaging flow cytometry platforms. These instruments work much like traditional flow cytometers; but additionally, an image of each event or cell is acquired, providing additional information on the spatial location of any fluorescent stainings employed. Typically, these instruments are equipped with 3–6 lasers and permit up to 12 channels of fluorescence data to be acquired alongside brightfield and darkfield images, thus enabling the high-content analysis of cells in suspension. In this way, imaging flow cytometry platforms allow the capture of high resolution images of 10000–20000 cells within minutes. Using an ImageStream X flow cytometer Rodrigues et al. (13) have shown that imaging flow cytometry can be used to effectively assess and score radiation induced MN in the cytokinesis blocked MN (CBMN) assay in primary human lymphocytes. However, the potential of the compact, more transportable and affordable FlowSight® imaging flow cytometer for scoring chemically induced MN *in vitro* in the CBMN and MN assay remains unexplored. To this end, here we evaluate the FlowSight® platform for the assessment of *in vitro* MN following cytokinesis block in the human lymphoblastoid cell lines TK6 and MCL-5 treated with known DNA damaging chemicals. These two P53 competent human lymphoblastoid cell lines were chosen on the basis that the TK6 cells are widely employed choice of cell line in both industry and academia due to their noted suitability in the OECD test guideline for the *in vitro* micronucleus assay (1). Similarly, the MCL-5 cell line is also frequently employed due to its stable expression of active cytochrome P450 metabolic enzymes that are vital for the activation of certain test articles (14). Manually scored MN frequencies derived from the images captured using FlowSight® are compared to the MN scores obtained from light microscopy to directly assess the reproducibility of the results from the two approaches. Our findings therefore represent an important first step towards the development of a high-throughput imaging flow cytometry based approach to compound screening for induced DNA damage via the MN assay facilitated using the more affordable FlowSight® imaging cytometry platform.

Materials and Methods

Chemicals

Methyl Methane Sulfonate (CAS no. 12925), Carbendazim (CAS no. 10605-21-7) and Benzo[a]pyrene (B[a]P) (CAS no. 50-32-8) were purchased from Sigma Aldrich, UK.

Cell lines and treatment

Human lymphoblastoid TK6 and MCL-5 cells were obtained from American Type Culture Collection (ATCC), Manassas, VA, USA. TK6 cells were cultured in RPMI 1640 media (Gibco, Paisley, UK), supplemented with 1% Pen/Strep (100 U/mL Penicillin and 100 µg/mL Streptomycin) and 10% heat inactivated horse serum (Gibco, Paisley, UK). MCL-5 cells were culture in RPMI 1640 (Gibco, Paisley, UK), supplemented with 10% horse serum, 1% L-glutamine (Gibco, Paisley, UK) and hygromycine-B. Cells were seeded at 2×10^5 cells in 25 cm^2 flask (Fisher brand), incubated at 37°C for 1.5–2 cell- cycles in the presence of MMS, Carbendazim and B[a]P.

Cytotoxicity and cytostasis

Relative Population Doubling (RPD) was used to estimate the highest dose to be included based on cytotoxicity. The 50 ± 5% reduction in percentage RPD was used to estimate highest tested concentration in accordance with the recommendation of the Organisation for Economic Co-operation and Development (1). Cell counts were determined automatically using a Coulter counter (Beckman Coulter Inc.). The %RPD calculations were made as follows:

$$\%\mathrm{RPD} = \frac{\text{Number of population doubling in treated cultures} \times 100}{\text{Number of population doubling in the vehicle control}}$$

Population Doubling (PD) was calculated as follows:

$$\mathrm{PD} = \log\left\{\frac{\text{cell count after treatment}}{\text{cell count in the control}}\right\} / \log 2$$

Cytokinesis Block Micronucleus (CBMN) assay

The *in vitro* CBMN assay was used to study MN induction in both TK6 and MCL-5 cells treated with MMS, Carbendazim and B[a]P. Cells were incubated with 3–6 µg/ml Cytochalasin-B (Cyto-B) continuously for a period of 30 h. Following incubation, cells were harvested via centrifugation at 200×*g* for 10 min. The supernatant was aspirated and the pellet was re-suspended in 10 ml phosphate-buffered saline (PBS) (Gibco®). The samples were then fixed and stained for MN scoring using imaging flow cytometry and manual scoring.

The light microscopy manual scoring approach (gold standard)

In the case of manual scoring conducted by light microscopy, 100 µl of cell suspension was centrifuged (Cytospin™ centrifuge) onto polished glass slides, fixed in 90% ice cold methanol for 10 min and

air dried at room temperature. Air dried slides were stained in 4% Giemsa solution (VWR International Ltd., Poole, UK) at room temperature. Giemsa stained slides were washed in Gurr buffer (Thermo Fisher Scientific) (pH 6.8), air dried and a cover slip was mounted on these slides using DPX mounting solution. The MN scoring was carried out using a 100× magnification objective on a light microscope (Olympus BX 51). Cells with two circular nuclei, non-overlapping, evenly stained and confined within the cytoplasmic boundary of the cell were scored as bi-nucleated cells. MN that were circular/oval, 1/3-1/16 the size of main nuclei and not overlapping the main nucleus of the bi-nucleated cells were included in the overall MN scores (15). The MN frequency per dose was obtained by manually assessing a total of 3000 bi-nucleated cells obtained across three experimental replicates.

FlowSight® analysis

For the imaging flow cytometric analyses, post 1.5–2 cell-cycle treatment, the PBS was removed and the cells were fixed using BD FACS™ lysis solution (CAS- 349202). Two millilitres of the fixative was added to each pellet followed by 12 min incubation at room temperature. Fixed cells were then washed, centrifuged at 200×*g* for 10 min before discarding the supernatant and processing for staining. Nuclei and MN were stained using 0.05 mM DRAQ5™ (CAS-564902, BD Biosciences) and were incubated for 30 min at room temperature prior to image acquisition using FlowSight®.

A 488 nm laser on FlowSight® (Amnis, part of EMD Millipore) was used to excite the DRAQ5 stained cells and images were captured automatically using the preinstalled INSPIRE®3.0 software. For image acquisition, 80 µl of cell suspension was processed on FlowSight®, with brightfield images captured alongside DRAQ5 fluorescence images of nuclei and MN via the 20× objective. The bright field image Aspect Ratio and Area parameters of the cells were then used to gate out debris and dead cells and to isolate the single cell population. Subsequently, cells acceptably within focus were further isolated by line scan gradient feature (brightfield gradient RMS). A total of 20 000 images of single, in-focus were captured on FlowSight® per dose/experimental replicate.

Prior to MN scoring, raw image files (.rif) obtained using INSPIRE® version 3.0 software were converted to Compensated Image Files (.cif) and Data Analysis Files (.daf) using identical settings via batch processing with template file in the manufacturer's IDEAS software (v5.0). An overlay of DRAQ5 fluorescence with the brightfield was then used for scoring and to assess that MN events lay within the cytoplasmic boundary of the parent cell. These overlaid composite images were then manually scored to classify cells based on their morphology as mono-, bi- or tri-nucleates with and without micronuclei. A total of 3000 bi-nucleated cells with two circular nuclei, displaying similar DRAQ5 staining characteristics and non-compromised cytoplasmic membrane were scored to evaluate the MN frequency. MN scoring within the bi-nucleated cells was carried out by adopting the criteria designed for slide based scoring (15). Only MN that were labelled with DRAQ5, were circular/oval, 1/3-1/16 the size of main nuclei of the bi-nucleated cells and were within the cytoplasmic boundary of the parent bi-nucleated cells were included in the final MN scores.

Statistical analysis

As necessary, data were $\log_{10}$ transformed to achieve a normal distribution (assessed via the Shapiro-Wilk Normality Test) with the homogeneity of within-dose variance further assessed by Bartlett Test. The Bonferroni test for outlier's was also conducted. If the transformed data passed these trend tests then the 1-sided Dunnett's test was used to identify the no- and the lowest-observed genotoxic effect levels (NOGEL and LOGEL, respectively). Where the data failed these trend tests, then the 1-sided Dunn's test was used to assess response significance relative to control according to the guidance laid out in (16).

Benchmark dose (BMD) analysis was carried out using 'defined' as covariate, with 'study' by which compound, scoring platform and cell line were used. PROAST software version 63.3 was used, and the data were fitted using both the exponential and Hill nested model families that are recommended by the European Food Safety Agency for the analysis of continuous toxicological dose-response data (17). PROAST uses the likelihood ratio test to assess whether inclusion of additional model parameters results in a significant improvement in model fit. Increasingly complex models with more parameters were only accepted if the difference in the log-likelihood exceeded $P < 0.05$. This permitted the establishment of which model parameters could be considered constant across subgroups in the combined datasets. As in earlier work, it was assumed that the shape parameters for maximum response (parameter c) and log steepness (parameter d) were constant in each analysis, while parameters for background response (parameter a), potency (parameter b) and var (i.e. within-group variation were examined for covariate dependency. (18,19). Using this approach, BMD lower and upper 90% confidence intervals (BMDL and BMDU) were defined and plotted to provide a quantitative, visually intuitive potency ranking for chemicals (20). A critical effect size (CES; also known as benchmark response, BMR) of 10% was used in all presented analyses (21).

Results

Here, we set out to investigate whether FlowSight® is a viable platform for the detection of chemically induced MN events *in vitro* using the human lymphoblastoid cell lines TK6 and MCL-5. Figure 1 clearly shows that with the FlowSight® platform, scorable, mono-nucleated, bi-nucleated, tri-nucleated and tetra-nucleated cells with or without MN can be captured accurately, without the need to lyse cells for MN assessment as is typically a requirement with conventional flow cytometry based approaches. Overall, confidence in MN scoring is vastly improved by being able to easily visualise every cell collected. The creation of an overlay of bright field/DRAQ5 images is extremely useful, as this helps to eliminate the subjectivity issues that arise with MN scoring with platforms where MN identification is conducted in the absence of cytoplasmic stain (e.g. is the parent cell a true bi-nucleate? Does the MN event truly correspond to the cell being scored or to its neighbour? etc.). Furthermore, visual inspection of the composite images enables the user to differentiate true MN events from equivocal/false positive events (e.g. difference in staining intensity of MN and the parent nuclei and size based differences between tri-nucleated cells and MN).

FlowSight® derived MN scores are comparable to the 'gold standard' light microscopy approach

The background levels of MN induction (i.e. in the zero dose controls) detected in the CBMN assay using FlowSight® were found comparable to manual MN frequencies using light microscopy based scoring, irrespective of the cell lines under investigation (Figure 2). Furthermore, the mean MN responses were comparable across the scoring platforms in TK6 cells for both MMS and Carbendazim treatment (Figure 2A/B). In the cells treated with MMS, both systems detected a significant ($P < 0.05$) increase in MN induction in response to 1.25, 2.5 and 5 µg/ml doses after 1.5–2 cell-cycle treatment. Both platforms also identified a significant ($P < 0.05$) increase

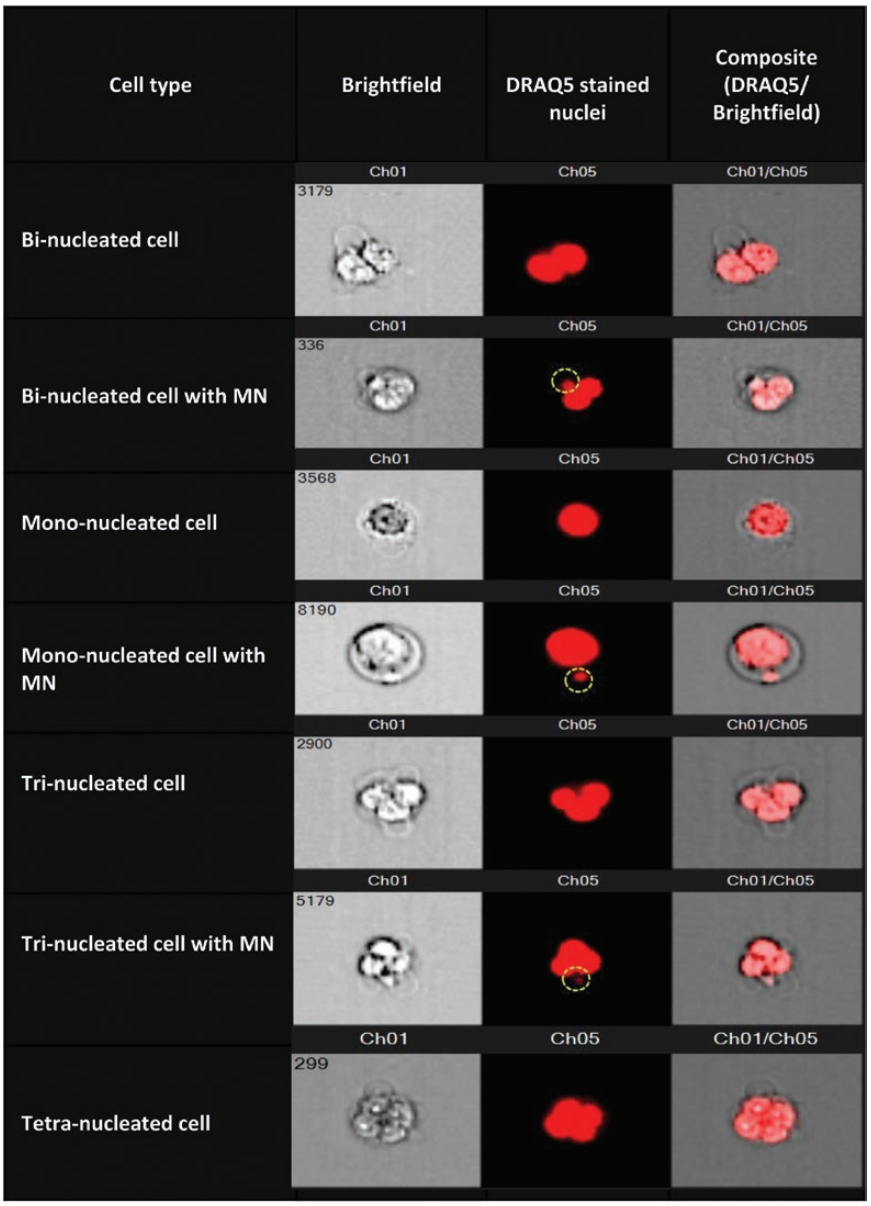

Figure 1. Example of cell images captured by FlowSight® imaging cytometry and manually classified as mono-nucleated, bi-nucleated, tri-nucleated and tetra-nucleated cells with or without MN. The left-most panel denotes cell classification, then moving right-wards, brightfield images, nuclear fluorescence (DRAQ5) and composite image overlay (brightfield/DRAQ5) are shown. MN events are highlighted by the yellow circles.

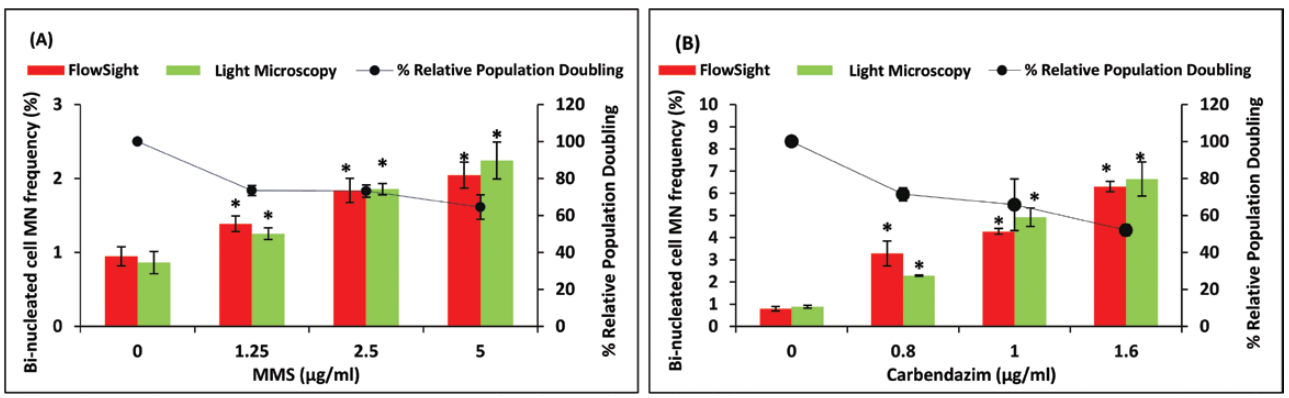

Figure 2. Comparison of the MN responses manually scored using images collected by FlowSight® imaging cytometry (black) and by conventional light microscope based manual scoring (white) in TK6 cells treated with MMS (A) and Carbendazim (B) following 1.5–2 cell-cycle treatment. (* indicates a significant increase in the MN formation over the control ($P < 0.05$)). Error bars represent mean ± SD ($n = 3$).

in MN for 0.8, 1 and 1.6 µg/ml Carbendazim doses following similar treatment regime. Again, the FlowSight® MN frequencies were in excellent concordance with the MN responses observed using conventional manual scoring by light microscopy.

Both MN scoring platforms also detected a significant ($P < 0.05$) increase in MN induction using the metabolically competent (i.e. expressing five cDNA that encode metabolic activating enzymes) (14) MCL-5 cells following 1.5–2 cell-cycle treatment (Figure 3). A significant ($P < 0.05$) increase in the MN induction was also observed in response to the 6.3 µg/ml dose of B[a]P using FlowSight®. Both the 0.75 and 6.3 µg/ml B[a]P concentrations were identified to cause a significant ($P < 0.05$) increase in MN when scored by traditional light microscopy.

Each of the analyses presented in Figure 3–4 indicated that the manually derived FlowSight® MN scores were in excellent concordance with those obtained in the comparative, manually scored light microscopy studies. To assess the different compound's potency ranking, as well as the degree of concordance across the techniques quantitatively, the BMD_{10} was calculated from the dose-response data for each study (i.e. chemicals, cell line and scoring method) using both the Hill and exponential model families (Figure 4). In each instance, the plotted BMD confidence intervals showed considerable overlap between scoring methods for each chemical, indicating good concordance across the FlowSight® and conventional light microscopy scoring techniques. The non-overlapping confidence intervals established between chemicals also allowed a potency ranking to be established from the data in order of potency of: Carbendazim (TK6)>MMS (TK6)≥B[a]P (MCL-5) (20).

Discussion and Conclusion

The proof-of-concept data provided here shows that the imaging flow cytometry based CBMN assay has the potential to be used to assess the genotoxicity of chemical compounds in immortalised human cell lines in addition to monitoring MN events in peripheral blood mononuclear cells for radiation dosimetry purposes as shown previously (13). We also show that the derived dose-response data were in excellent concordance across the imaging cytometry and light microscopy platforms. Here, the BMD approach was used to compare data from the two scoring methods as there is a growing consensus that this method constitutes a robust approach for comparing potency estimates arising across different covariates (e.g. compounds, cell lines, time points etc.) (19,20). Recently, the combined BMD-covariate approach has similarly been used to assess the comparability of potency estimates arising across different variants (e.g. employing different rodent species and/or different reporter transgenes) of the transgenic rodent gene mutation test (23). The approach has also been used to compare compound potency estimates arising from data collected by different laboratoreis during the Japanese *in vivo* ring trial for the Pig-a gene mutation assay and the transgenic mutation system (22).

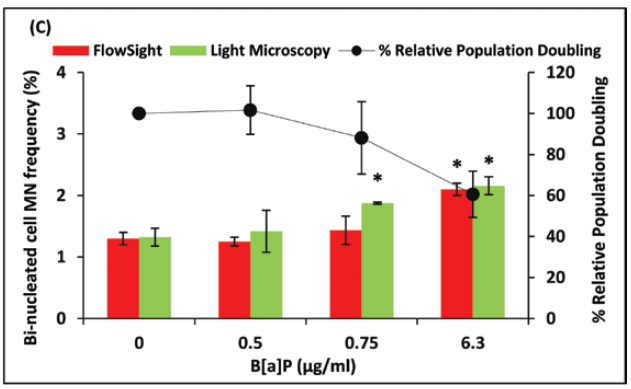

Figure 3. Comparison of the MN responses manually scored using images collected by FlowSight® (black) and light microscope based manual scoring (white) in MCL-5 cells treated with B[a]P for 1.5–2 cell cycles. (* indicates a significant increase in the MN formation over the control ($P < 0.05$)). Error bars represent mean ± SD ($n = 3$).

Here, FlowSight® (imaging flow cytometry) based MN scoring was carried out in unlysed cells, giving it an advantage over standard flow cytometric platforms that often require cell lysis for MN assessment. The strategy to assess MN induction in the absence of cell lysis adheres to OECD recommendations, whereby MN scoring should ideally be conducted in cells with intact cytoplasmic membranes (12). Moreover, visual inspection of the cellular images helps to reject apoptotic cells and permits correct identification of bi-, tri- and multi-nucleated cells with and without MN, which otherwise are suspected to influence MN scoring upon lysis with the conventional flow cytometric method (3). Standard flow cytometry based MN scoring is also limited to mono-nucleated cells, whereas the approach described here is suitable for MN scoring both with or without cytokinesis block, with many laboratories favouring one approach over the other. In addition to this, the FlowSight® approach allows every cell and MN event to be visualised and recorded automatically during the data acquisition process. When compared to manual scoring using light microscopy, FlowSight® image-sets of 20 000 cells can be acquired within minutes, providing statistically relevant populations of cells for downstream analysis. The images can be archived, accessed, could be quickly re-scored as better-trained automated algorithms become available and can be submitted to regulatory authorities or scientific journals to validate findings as required.

During the current project, we used the FlowSight® imaging cytometer (Amnis, part of Merck Millipore) and captured images using the standard-equipped 20× objective. The image resolution could be further improved by using a higher magnification objective (e.g. 40× objective). However, the 20X objective proved effective in the initial proof-of- concept work presented here. The FlowSight® imaging cytometer was also of interest to us as previous work has used the more expensive 'ImageStreamX' series imaging cytometers. The FlowSight® model is designed to be more compact and affordable and thus our successes here are important, as the FlowSight® is more within reach of a wider range of research and industrial laboratories.

It is important to note that the speed and objectivity of MN scoring could be further enhanced through the development of a fully automated algorithm for MN scoring. We propose that supervised machine learning is the ideal approach for such image analysis based classifications, and we are working towards such an approach at the current time, using the manually classified events established here as the 'ground truth' to train and validate the algorithm. A further advantage of using such an approach in comparison to the traditional object-based classifiers used to-date is that accuracy can be improved each time new data sets are available for analysis. This approach also has the potential to be more flexible in detecting events that are chemical specific, for example, some current classifiers only score cells with perfectly circular nuclei, whereas aneugen exposure can increase the number of cells with non-circular nuclei that are none-the-less still scorable (3). Furthermore, there is also the potential to introduce additional

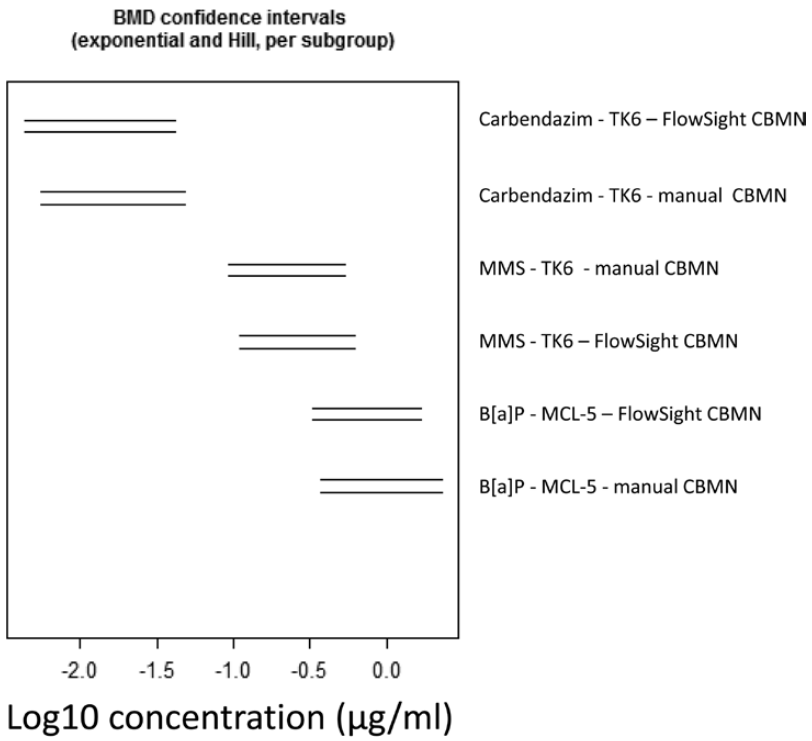

Figure 4. Plotted benchmark dose (BMD) $BMDL_{10}$-$BMDU_{10}$ confidence intervals, with those derived using the fitted exponential model (top horizontal line) and the Hill model (bottom horizontal line) for each study. The BMD analysis was conducted with 'study' (i.e. compound, scoring method and cell line) as covariate to compare compound potency and to assess the reproducibility of the dose-response data arising across the two scoring platforms (i.e. light microscopy or FlowSight® image cytometry). The benchmark response (BMR) used was 10%. The BMD analyses, underlying dose-response data and fitted BMD models are presented in Supplementary Figures S1 and S2. Carb = Carbendazim; MMS = Methyl Methansulfonate; B[a]p = Benzo[a]Pyrene; CBMN = cytokinesis blocked micronucleus assay.

markers (e.g. antibody labels) to provide additional information on the mechanism for MN induction as clastogenic or aneugenic (e.g. γH2AX or phosphorylated histone H3) (23,24).

We suggest that an inter-laboratory trial is essential to test the reproducibility and transferability of the experimental protocol, and once fully developed the automated machine learning based MN scoring algorithm as well. We are moving forward with both of these goals in mind, but this initial paper focusses on providing proof-of-concept that chemically induced MN events can be captured and scored using FlowSight®, in different cell lines, following exposure to aneugens and clastogens, and that the events recorded by imaging flow cytometry align with manual scores recorded by gold standard light microscopy. This proof-of-concept has been realised, and the supervised machine learning approach based on our developing ground truth will now be fully developed and validated using various cell lines and test articles with varying modes-of-action via inter-laboratory trial.

Supplementary data

Supplementary Figures S1 and S2 are available at *Mutagenesis* Online.

Acknowledgements

We would like to thank to the Life Science Bridging Fund within the Life Science Research Network Wales (LSBF/R3-007) and AgorIP (WEFO) who provided funding for the project. We are also very grateful to Dr R.Wilkins and Dr L. Beaton-Green at Health Canada for sharing their knowledge and expertise.
Conflict of interest statement: None declared.

References

1. OECD. (2014) *OECD TG487 Guideline for the Testing of Chemicals, In Vitro Mammalian Cell Micronucleus Test*. Organisation for Economic Cooperation and OECD, Paris. doi:10.1787/9789264244438-en.
2. ICHS2(R1). (2012) *International Conference on Harmonisation; Guidance on S2(R1) Genotoxicity Testing and Data Interpretation for Pharmaceuticals Intended for Human Use*; availability. Notice. Fed Regist 77, 33748–33749.
3. Verma, J. R., Rees, B. J., Wilde, E. C., Thornton, C. A., Jenkins, G. J. S., Doak, S. H. and Johnson, G. E. (2017) Evaluation of the automated MicroFlow® and Metafer™ platforms for high-throughput micronucleus scoring and dose response analysis in human lymphoblastoid TK6 cells. *Arch. Toxicol.*, 91, 2689–2698.
4. Decordier, I., Papine, A., Plas, G. *et al.* (2009) Automated image analysis of cytokinesis-blocked micronuclei: an adapted protocol and a validated scoring procedure for biomonitoring. *Mutagenesis*, 24, 85–93.
5. Verhaegen, F., Vral, A., Seuntjens, J., Schipper, N. W., de Ridder, L. and Thierens, H. (1994) Scoring of radiation-induced micronuclei in cytokinesis-blocked human lymphocytes by automated image analysis. *Cytometry*, 17, 119–127.
6. Avlasevich, S. L., Bryce, S. M., Cairns, S.E. and Dertinger, S.D. (2006) In vitro micronucleus scoring by flow cytometry: differential staining of micronuclei versus apoptotic and necrotic chromatin enhances assay reliability. *Environ. Mol. Mutagen.*, 47, 56–66.
7. Rossnerova, A., Spatova, M., Schunck, C. and Sram, R. J. (2011) Automated scoring of lymphocyte micronuclei by the MetaSystems Metafer image cytometry system and its application in studies of human mutagen sensitivity and biodosimetry of genotoxin exposure. *Mutagenesis*, 26, 169–175.
8. Doherty, A. T., Hayes, J., Fellows, M., Kirk, S. and O'Donovan, M. (2011) A rapid, semi-automated method for scoring micronuclei in mononucleated mouse lymphoma cells. *Mutat. Res.*, 726, 36–41.

9. Bolognesi, C., Balia, C., Roggieri, P., Cardinale, F., Bruzzi, P., Sorcinelli, F., Lista, F., D'Amelio, R., and Righi, E. (2011) Micronucleus test for radiation biodosimetry in mass casualty events: evaluation of visual and automated scoring. *Radiat. Meas*., 46, 169–175.
10. Seager, A. L., Shah, U. K., Brüsehafer, K. *et al.* (2014) Recommendations, evaluation and validation of a semi-automated, fluorescent-based scoring protocol for micronucleus testing in human cells. *Mutagenesis*, 29, 155–164.
11. Bryce, S. M., Bemis, J. C., Avlasevich, S. L. and Dertinger, S. D. (2007) In vitro micronucleus assay scored by flow cytometry provides a comprehensive evaluation of cytogenetic damage and cytotoxicity. *Mutat. Res*., 630, 78–91.
12. Fenech, M., Kirsch-Volders, M., Rossnerova, A. *et al.* (2013) HUMN project initiative and review of validation, quality control and prospects for further development of automated micronucleus assays using image cytometry systems. *Int. J. Hyg. Environ. Health*, 216, 541–552.
13. Rodrigues, M. A., Beaton-Green, L. A., Kutzner, B. C. and Wilkins, R. C. (2014) Automated analysis of the cytokinesis-block micronucleus assay for radiation biodosimetry using imaging flow cytometry. *Radiat. Environ. Biophys*., 53, 273–282.
14. Crespi, C. L., Gonzalez, F. J., Steimel, D. T., Turner, T. R., Gelboin, H. V., Penman, B. W. and Langenbach, R. (1991) A metabolically competent human cell line expressing five cDNAs encoding procarcinogen-activating enzymes: application to mutagenicity testing. *Chem. Res. Toxicol*., 4, 566–572.
15. Fenech, M., Chang, W. P., Kirsch-Volders, M., Holland, N., Bonassi, S. and Zeiger, E.; HUman MicronNucleus project. (2003) HUMN project: detailed description of the scoring criteria for the cytokinesis-block micronucleus assay using isolated human lymphocyte cultures. *Mutat. Res*., 534, 65–75.
16. Johnson, G. E., Soeteman-Hernández, L. G., Gollapudi, B. B. *et al.* (2014) Derivation of point of departure (PoD) estimates in genetic toxicology studies and their potential applications in risk assessment. *Environ. Mol. Mutagen*., 55, 609–623.
17. Guidance, E. F. S. A. (2009) Guidance of the scientific committee on use of the benchmark dose approach in risk assessment. *EFSA Journal*, 7, 1150.
18. Slob, W. and Setzer, R. W. (2014) Shape and steepness of toxicological dose-response relationships of continuous endpoints. *Crit. Rev. Toxicol*., 44, 270–297.
19. Wills, J. W., Johnson, G. E., Doak, S. H., Soeteman-Hernández, L. G., Slob, W. and White, P. A. (2016) Empirical analysis of BMD metrics in genetic toxicology part I: in vitro analyses to provide robust potency rankings and support MOA determinations. *Mutagenesis*, 31, 255–263.
20. Wills, J. W., Long, A. S., Johnson, G. E., Bemis, J. C., Dertinger, S. D., Slob, W. and White, P. A. (2016) Empirical analysis of BMD metrics in genetic toxicology part II: in vivo potency comparisons to promote reductions in the use of experimental animals for genetic toxicity assessment. *Mutagenesis*, 31, 265–275.
21. Bemis, J. C., Wills, J. W., Bryce, S. M., Torous, D. K., Dertinger, S. D. and Slob, W. (2016) Comparison of in vitro and in vivo clastogenic potency based on benchmark dose analysis of flow cytometric micronucleus data. *Mutagenesis*, 31, 277–285.
22. Johnson, G. E., Yamamoto, M., Suzuki, Y. *et al.* (2016) Measuring reproducibility of dose response data for the Pig-a assay using covariate benchmark dose analysis. *Mutat. Res*., 811, 135–139.
23. Bryce, S. M., Bernacki, D. T., Bemis, J. C. *et al.* (2017) Interlaboratory evaluation of a multiplexed high information content in vitro genotoxicity assay. *Environ. Mol. Mutagen*., 58, 146–161.
24. Wilkins, R. C., Rodrigues, M. A. and Beaton-Green, L. A. (2017) The application of imaging flow cytometry to high-throughput biodosimetry. *Genome Integr*., 8, 7.